# Light-induced Suppression on Forming Secondary Phases in FA-rich Perovskite

Chang-En Tsai

A thesis

submitted in partial fulfillment of the

requirements for the degree of

Master of Science

In Chemical Engineering

University of Washington

2021

Committee:

Hugh W. Hillhouse

David A. C. Beck

Program Authorized to Offer Degree:

Chemical Engineering

University of Washington

## Abstract

Light-induced Suppression on Forming Secondary Phases in FA-rich Perovskite

Chang-En Tsai

Chair of the Supervisory Committee:

Hugh W. Hillhouse

Department of Chemical Engineering

Investigating the environmental factors that affect the degradation pathway in hybrid organic-inorganic perovskites such as $(MA,FA,Cs)Pb(I,Br)_3$ is important for improving their stability. In this work, we show that illumination with above bandgap stabilizes FA-rich perovskites films. Bright-field and dark-field microscopy images were collected in-situ during the degradation and showed that FA-rich perovskites aged under illumination formed less secondary phases than control samples aged in the dark. These secondary phases were confirmed to be intermediate products of degradation by X-ray diffraction. The light-induced stabilization in perovskites films are only observed in FA-rich perovskites. We investigated the effect on perovskites structure resulted from alloying different cations in the films using Williamson-Hall analysis and the impact on light absorption by analyzing the below bandgap absorption states (Urbach tails). Therefore, this work demonstrates the phenomenon of light slowed down the formation of intermediate degradation products, and resulted in more stable perovskite structure.

## 1. Introduction

Hybrid organic-inorganic perovskites ($ABX_3$ , A = methylammonium (MA), formamidinium (FA), Cs; B = Pb,; X = I, Br) have become one of the most promising materials in the photovoltaics(PV) field based on its tremendous improvement on power conversion efficiency (PCE), increasing from 3.8%[1] to 25.2%[2], and the low temperature solution-processing ability greatly reduce fabrication cost, allowing it to become a competitive candidate in the PV field[3]. Besides, another attractive property of perovskites as PV active layer is the flexibility on tuning the bandgap(Eg) by alloying different A-site cation or halide into perovskites[4,5].

Although having many significant advantages, there are disadvantages to perovskites as well. They contain the toxic element Pb[6] and its instability leads to it having a short lifetime compared to Si based solar cells, limiting its possibility of being commercialized. Therefore, the research has gradually switched from improving PCE to investigating the degradation pathway in order to obtain a longer lifetime of perovskites recently, and even aim for passing the stability test for commercially available PV[6]. Extrinsic factors, illumination[7–9], humidity[10–12], oxygen[8,13], and heat[14,15] induced degradation pathway in perovskites are being studied and reported in the PV field[16]. Other than investigating in extrinsic factors induced degradation pathway in perovskites, compositional engineering by A-site cation and X-site anion has been identified as one of the major methods in optimizing the stability and optoelectronic properties[17,18].

Compositional engineering in perovskites resulted in great improvement in stability[19] ,but due to the low temperature annealing fabrication process and its polycrystalline nature[20], the formation of defects in perovskites crystalline structure is unavoidable. Even though perovskites have superior defect tolerance, defects are still considered as a major factor which greatly affect the stability. Many studies have reported it as one of the major reasons which result in

photocurrent-voltage hysteresis in perovskites PV[21] and vulnerable sites for water and oxygen induced degradation pathways[22]. Therefore, to achieve more stable perovskites PV devices, a more precise and deeper understanding of its compositions, defects and degradation pathway is of great significance.

In this work, we tracked the optoelectronic properties, and crystalline structural stability of (MA,FA,Cs)Pb(I,Br)$_3$ perovskites thin films to understand the degradation of perovskites through aging experiment under ambient environment with 0.25 Sun illumination and in the dark respectively. We observed the UV-vis-NIR spectral data of thin films are consistent with reported light-induced degradation pathway in perovskites[9]. Yet, we found that for (FA,Cs)PbI$_3$ perovskites which aged under 0.25 Sun illumination formed less secondary phases than the control samples aged in the dark from our microscopy bright-field (BF) and dark-field (DF) images. This result indicated the α-(FA,Cs)PbI$_3$ phase perovskites structure is relatively more stable under illumination than in the dark. To our knowledge, this phenomenon has not been reported yet. Besides, from X-ray diffraction (XRD) patterns of thin films, we found secondary phases XRD peaks only appeared in (FA,Cs)PbI$_3$ which aged in the dark. The observed degraded intermediate products are consistent with the reported degradation pathways of (FA,Cs)PbI$_3$ perovskites that moisture drives cubic perovskites phase to hexagonal phase then hydrated phases[23]. Besides, we observed no secondary phases formed in (FA,Cs)Pb(I,Br)$_3$ perovskites, indicating that incorporation of Br can effectively stabilize the perovskites and stopping the formation of secondary phases and this observation is consistent with the reported studies[24,25]. Furthermore, we discovered the sub-bandgap absorption shares same increasing trend with the microstrain from our Urbach tails ($E_u$) and Williamson-Hall analysis. $E_u$ are affected by many factors, such as disordered

material[26], thermal disorder[27], and internal electric field-induced absorption,[28] hence light-induced stabilization on perovskites phase is strongly related to them.

## 2. Experimental Methods

### 2.1 Perovskites Film Deposition

Perovskites thin films were prepared on 15mm square glass substrate which were cleaned with a four-step procedure by sonicating for 10 minutes each in this order (1) Alconox and DI water, (2) DI water, (3) acetone, and (4) 2-propanol. Glass substrates then were transferred to Ar plasma cleaner and cleaned for 10 minutes. All precursor inks were prepared by dissolving stoichiometric MAI, FAI, CsI, $PbI_2$, $PbBr_2$ at 1M in 1/1 vol/vol N-methyl-2-pyrrolidone (NMP)/dimethylformamide(DMF), and stirred for 30 mins at 25$^{o}$C, then left over night. MAPbI and MAFACsPI ink were spin coated at 4000 rpm for 45 sec, then immersed in a diethyl ether (DEE) antisolvent bath for 60 sec. FACsPI and FACsPIBr precursor inks were spin coated at 4000 rpm for 45 sec, then 0.58mL of toluene dispensed at 12 sec remaining over 5 sec. All spin coated thin films were then transferred to hot plate and annealed at 100$^{o}$C for 10 min. All ink preparation, spin coating, and annealing procedures were carried out in a $N_2$-filled glovebox.

### 2.2 Film Characterization

UV-Vis-NIR was collected on a Perkin-Elmer 1050 UV/VIS/NIR spectrometer equipped with a Peltier-cooled InGaAs detector for IR, PbS detector for NIR, and a tungsten-halogen lamp as light source and absorption data was taken in an equipped integrated sphere. To collect the absorption data, the films were deposited on soda lime glass substrates which sharing same method

as mentioned above in film deposition. UV-Vis-NIR data can also be refined by using the absorption information one can determine sub-bandgap absorption from $E_u$ analysis.

X-ray diffraction (XRD) was collected on the films with a Bruker D8 Discover instrument equipped with Pilatus 100K large-area 2D detector and a Cu anode microfocus X-ray source (wavelength 1.542Å, Kα radiation). The X-ray beam size was defined with a 0.5mm collimator. XRD spectral data can also be refined by using the peak information one can determine microstrain in the lattice structure from Williamson-Hall analysis.

Scanning electron microscope (SEM) was applied with a FEI Sirion XL30 by an electron beam with an accelerating voltage of 5 kV. To avoid charging effects, 4 nm of Pt coating was sputtered onto all perovskites films prior to imaging.

Microscopy images were taken by a Zeiss Axioscope A1 with a Canon EOS Rebel T7i camera and a Zeiss 20x objective with bright-field and dark-field capability. Optical images were taken by Apple Iphone SE camera, and images are presented without further editing.

2.3 Aging Experiment Setup

Degradation experiments on perovskites thin films were conducted in a self-built environmental chamber which made of acrylic with controlled atmosphere at room temperature. Relative humidity (RH) is controlled by attaching an ultrasonic humidifier and the dry air. By fixing the power output of humidifier and adjusting the flow rate of dry air to achieve the desired % of RH. Illumination is applied with a DLP diffused ring light panel from Smart Vision Lights, and the intensity of light source was calibrated with a Newport 91150 V Si reference diode to fix the light intensity at 0.25 Sun.

## 3. Results and Discussion

### 3.1 Optical Analysis of Perovskites Film

To qualitatively study the degradation in perovskites thin film, the UV-vis-NIR absorption and optical characterization for all perovskites thin films were carried out during the aging experiment. For this study, the composition of perovskites was $MAPbI_3$, $(FA_{0.83}Cs_{0.17})PbI_3$, $(FA_{0.83}Cs_{0.17})Pb(I_{0.86}Br_{0.14})_3$, and $(MA_{0.738}FA_{0.217}Cs_{0.045})PbI_3$. All samples were aged in air environment under 40% RH at room temperature, and one set of samples was kept under 0.25 Sun illumination and another set was kept in the dark.

For $MAPbI_3$ perovskites (Figure 1a), when exposed under 0.25 Sun illumination, it showed rapidly degradation on photoactive perovskites and totally degraded after 4 hours of aging. The color of perovskites sample obviously changed from dark brown to yellowish, other than optical characterization, UV-vis-NIR spectral data also showed the absorption dramatically decreased in between 780 nm and 520 nm (Figure 1a). Both these two characterizations are consistent with the reported degradation of perovskites, and the formation of degraded products $PbI_2$.[16]. However, no degradation was observed in control $MAPbI_3$ perovskites sample which aged in the dark until 66 hours of aging experiment. Our data confirmed and consistent with the reported result of illumination activated photo-oxidation[9,29] degradation pathway in perovskite and indicated $MAPbI_3$ perovskites are less stable under illumination than the control $MAPbI_3$ sample in the dark.

For $(MA_{0.738}FA_{0.217}Cs_{0.045})PbI_3$ perovskites aged under illumination (Figure 1c), the color of sample gradually changed from dark brown to pale brown along with the decreasing of UV-vis-NIR absorption in between 770 nm to 450 nm during 258 hours of aging experiment (blue trace). This result implied the decomposition of photoactive perovskites structure. On the other hand, for control $(MA_{0.738}FA_{0.217}Cs_{0.045})PbI_3$ sample aged in the dark, the color of sample also changed from

dark brown color to pale brown color along with the decrease of UV-vis-NIR absorption during 258 hours of aging experiment, however, it showed obviously darker than the control sample under illumination and with higher absorption in UV-vis-NIR spectral data shown in Figure 1c. This clearly illustrated the degradation rate of perovskites in dark is slower than under illumination.

Besides, the optical and UV-vis-NIR characterization for sample, $(FA_{0.83}Cs_{0.17})PbI_3$, and $(FA_{0.83}Cs_{0.17})Pb(I_{0.86}Br_{0.14})_3$ are presented in Figure 1b and Figure 1d. The UV-vis-NIR spectra of the pristine samples show different absorption onset at ~820nm for pure I and ~775nm for 86% of I and 14% of Br corresponding to their bandgap, ~1.51 eV and ~1.6 eV respectively. The difference in bandgap is resulted from higher content of Br in the perovskites structure.[30] The gradually decrease of UV-vis-NIR absorption in between ~600 nm and ~830 nm under illumination condition was observed yet did not show significant variation on the absorption spectral data which aged in the dark. The decrease of UV-vis-NIR absorption directly confirmed the degradation of perovskites, and proved perovskites underwent faster degradation under illumination than in the dark (Figure 1b, Figure 1d). This agrees with previous data from $MAPbI_3$ and $(MA_{0.738}FA_{0.217}Cs_{0.045})PbI_3$ perovskites samples, and further proved that perovskites are less stable under illumination than in the dark.

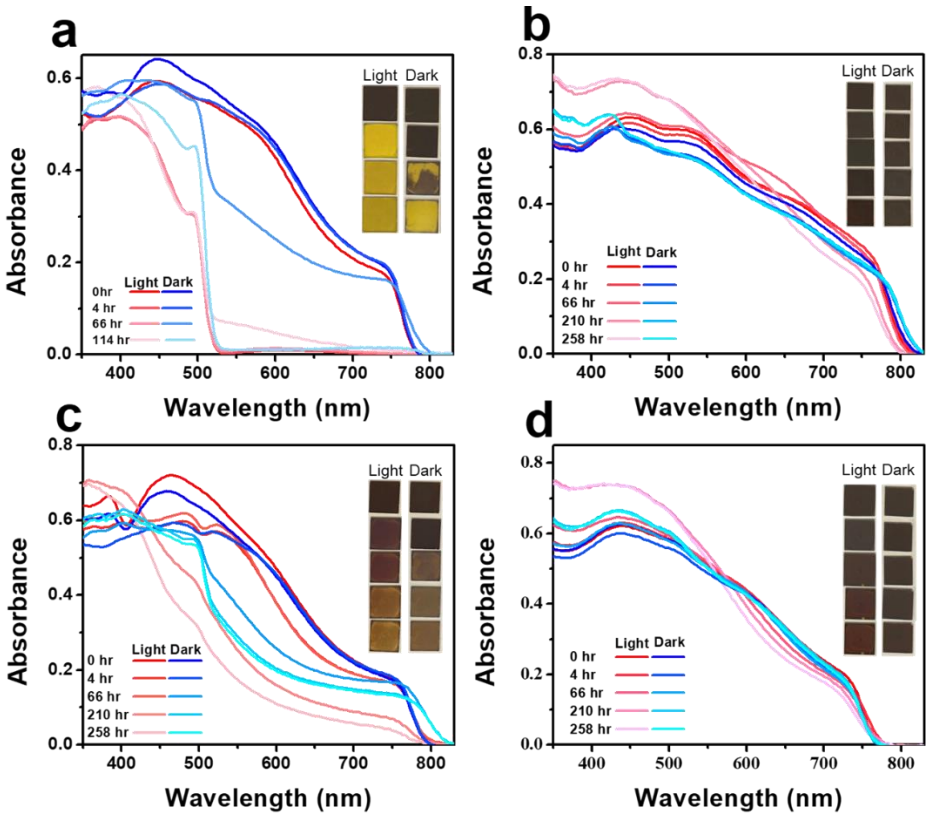


Figure 1. Optical and UV-vis-NIR characterization of spin-coated films. (a) $MAPbI_3$, (b) $(FA_{0.83}Cs_{0.17})PbI_3$, (c) $(FA_{0.83}Cs_{0.17})Pb(I_{0.86}Br_{0.14})_3$, (d) $(MA_{0.738}FA_{0.217}Cs_{0.045})PbI_3$

3.2 Structural Characterization of Perovskites Film

FA and Cs cations are common substitution in A-site of perovskites and have been reported to be incorporated into perovskites structure and greatly enhance the stability of perovskites[19]. We measured XRD and SEM on the spin-coated thin films for different compositions to investigate the crystalline structure and the phase purity of perovskites. Figure 2a shows $MAPbI_3$ perovskites formed tetragonal crystalline structure however other multiple cation alloy perovskites formed cubic phase crystalline structure. We noticed the XRD peak broadening in Figure 2a varies with compositions, and believe these differences are resulted from size and strain in the crystalline structure.

Strain in the crystalline structure occurs from lattice distortion, dislocations, or grain surface relaxation[31]. By applying Williamson-Hall[32] analysis from XRD pattern data will allow us to investigate the size and strain for each alloy, and the relative trend. In Figure 2b, the Williamson-Hall analysis result shows the microstrain of each alloy from the XRD pattern. From Williamson-Hall analysis result, the microstrain in $(FA_{0.83}Cs_{0.17})PbI_3$ is 120% higher than $MAPbI_3$, yet only 20% higher than $(FA_{0.83}Cs_{0.17})Pb(I_{0.86}Br_{0.14})_3$. The significant difference in microstrain in between $MAPbI_3$ and $(FA_{0.83}Cs_{0.17})PbI_3$ proved that FA and Cs are incorporated into A-site, and the increasing microstrain trend matches with the A-site ionic radii. Although A-site and X-site substitution could have different impacts on microstrain hence we analyzed $(FA_{0.83}Cs_{0.17})Pb(I_{0.86}Br_{0.14})_3$ microstrain by Williamson-Hall analysis as well, and the insignificant difference in microstrain in between $(FA_{0.83}Cs_{0.17})PbI_3$ and $(FA_{0.83}Cs_{0.17})Pb(I_{0.86}Br_{0.14})_3$ indicates that the X-site of perovskites has relatively small effect on microstrain in perovskites structure. In Figure 2c, the optical property of perovskites is characterized by UV-vis-NIR absorption. It has been reported that the bandgap of perovskites could be tuned by substituting A-site and X-site composition[30,33]. We noticed that the absorption of $(FA_{0.83}Cs_{0.17})PbI_3$ (Figure 2c) onset at approximately 1.56 eV and showing the lowest bandgap compare with other three alloys. This decreasing bandgap trend agrees with the reported result[34] and evidence FA and Cs are successfully incorporate into A-site. On the other hand, $(FA_{0.83}Cs_{0.17})Pb(I_{0.86}Br_{0.14})_3$ alloy shows highest

bandgap with approximately 1.64 eV. This result allowed us to confirm that Br is successfully incorporated into x-site.

Figure 2. Structural and optical characterization of spin-coated films. (a) XRD of perovskites samples. (b) Williamson-Hall analysis of A-site and X-site compositions. (c) UV-Vis-NIR absorption of perovskites samples

3.3 Morphological and Phase Purity Characterization of Perovskites Film

Compositional engineering by A-site and X-site substitution have been reported as a

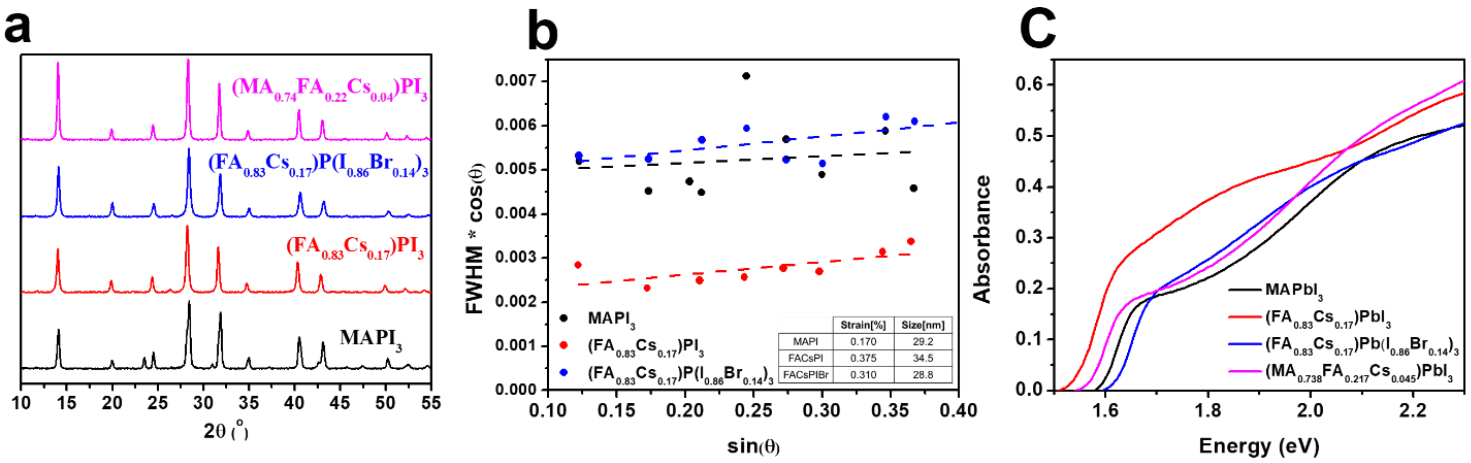


common method in optimizing the stability and the optoelectronic properties of perovskites[19,31,35]. Thus, the control of crystallization process is the key aspect for fabricating high quality and reproducible perovskites. To track the phase purity, top-view SEM images of pristine perovskites films were collected to inspect the morphology of fabricated samples. In Figure 3a, 3c, and 3d, the morphology and grain size of different composition of perovskites showed evenly distributed. In Figure 3b, we observed that there are secondary phases formed in $(FA_{0.83}Cs_{0.17})PbI_3$ perovskites. Despite we observed secondary phases in $(FA_{0.83}Cs_{0.17})PbI_3$ perovskites, from XRD spectral data

shown in Figure 2a, no secondary phases peak was detected. This result gives us confidence that secondary phases in $(FA_{0.83}Cs_{0.17})PbI_3$ are relatively trivial compared to perovskites phase.

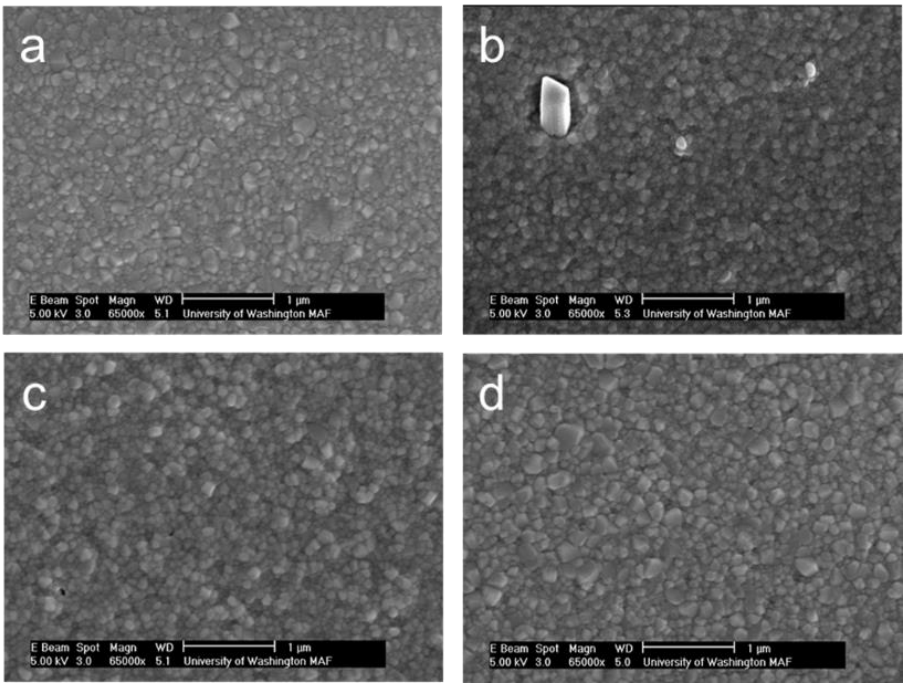


Figure 3. Morphological characterization of pristine spin-coated films. (a) $MAPbI_3$, (b) $(FA_{0.83}Cs_{0.17})PbI_3$, (c) $(FA_{0.83}Cs_{0.17})Pb(I_{0.86}Br_{0.14})_3$, (d) $(MA_{0.738}FA_{0.217}Cs_{0.045})PbI_3$

Many degradation pathways in FA-rich perovskites have been reported along with the intermediate secondary phases formation has being studied and presented in several reports[36]. Gratia et al. reported multiple phases in perovskites and the crystallization process of forming perovskites.[37] Moreover, Marchezi et al. demonstrated the degradation route in $(FA_{1-x}Cs_x)Pb(I_{1-y}Br_y)_3$ is related to the composition of perovskites, and each degradation route occurred with different intermediates and final products.[23] Thus, we believe the formation of secondary phases is intertwined with the degradation of perovskites and could be used as an indicator of degradation of perovskites. To track the secondary phases intensity variation during the aging experiment, we applied microscope with the capability of BF and DF on the spin-coated perovskites thin films.

For $(FA_{0.83}Cs_{0.17})PbI_3$ perovskites sample, secondary phases were observed at initial status, which consistent with our SEM data shown in Figure 3b. For control sample aged under 0.25 Sun illumination (Figure 4, top two rows), the needle-like secondary phases slightly increased after 66 hours of aging. In BF images (Figure 4, top first row), the secondary phases slightly increased after 16 hours of aging, and the trend of increasing secondary phases were also observed after 66 hours. In DF images (Figure 4, top second row), the white needle-like secondary phases structures are consistent with the result in BF images. For control $(FA_{0.83}Cs_{0.17})PbI_3$ sample which aged in the dark (Figure 4, bottom two rows), the needle-like secondary phases showed same increasing trend with the control sample aged under 0.25 Sun illumination (Figure 4, top two rows) during aging. In BF images (Figure 4, third row from top), we observed the secondary phases significantly increased after 16 hours of aging and showing the same increasing trend after 66 hours of aging. From DF images (Figure 4, bottom row), the white needle-like secondary phases showed same result we observed from BF images (Figure 4, third row from top). From Figure 4, we observed that the $(FA_{0.83}Cs_{0.17})PbI_3$ sample which aged under 0.25 Sun illumination (Figure 4, top two rows) although demonstrated increasing trend in secondary phases during the aging experiment, compared to the control sample aged in the dark (Figure 4, bottom two rows), illumination showed significantly effect on suppressing the formation of secondary phases in perovskites. On the other hand, the $(FA_{0.83}Cs_{0.17})PbI_3$ control sample aged in the dark, showed greatly increasing trend of secondary phases after 18 hours of aging. Thus, from these observations, we suppose that illumination can suppress the formation of secondary phases in FA-rich perovskites and stabilize the perovskites structure.

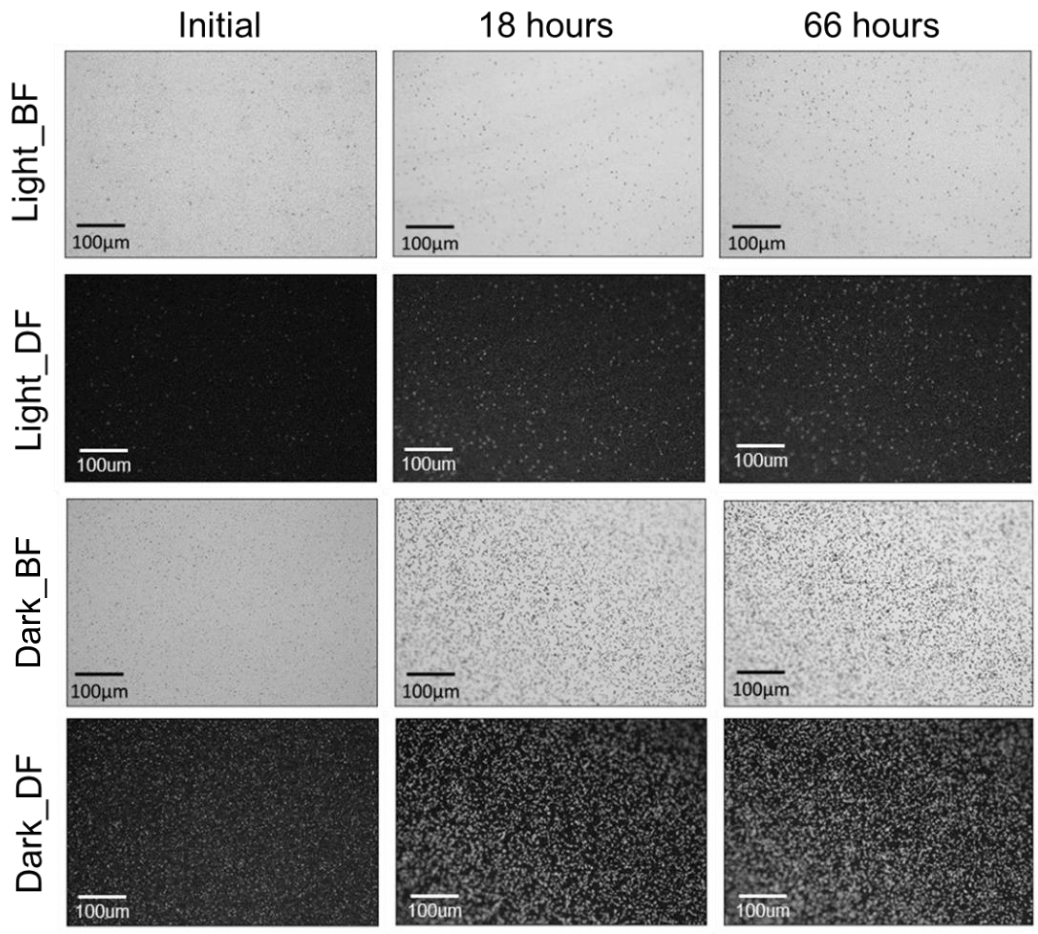


Figure 4. Secondary phases intensity tracking of $(FA_{0.83}Cs_{0.17})PbI_3$ perovskites during aging in ambient environment conditions (40% RH, 25°C)

For $(FA_{0.83}Cs_{0.17})Pb(I_{0.86}Br_{0.14})_3$ perovskites, the microscopy BF and DF images are shown in Figure 5. Both $(FA_{0.83}Cs_{0.17})Pb(I_{0.86}Br_{0.14})_3$ samples which aged in the dark and under illumination showed no secondary phases are formed at initial status. These images share the same result with our SEM images. For sample aged under 0.25 Sun illumination (Figure 5, top two rows), there are no secondary phases were observed in BF images (Figure 5, top row) after 66 hours of aging experiment. In DF images (Figure 5, second row from top), we observed no needle-like secondary phases were formed either. This result indicated that the phase purity of

$(FA_{0.83}Cs_{0.17})Pb(I_{0.86}Br_{0.14})_3$ sample remain similar with the initial status and proved light is stabilizing the perovskites cubic phase and suppressing the formation of secondary phases. On the other hand, for control sample which aged in the dark (Figure 5, bottom two rows), it clearly showed the formation of secondary phases during 66 hours of aging. From BF images which presented in third row from top of Figure 5, it obviously formed needle-like shape secondary phases after 18 hours of aging experiment. Besides, after aging in the dark for 66 hours, the needle-like shape secondary phases grew bigger, although these secondary phases were not clearly shown in DF images which presented at the bottom row of Figure 5. This result consistent with the sample $(FA_{0.83}Cs_{0.17})PbI_3$ (Figure 4) showing that illumination suppressed the formation of secondary phases and stabilized the perovskites crystalline structure.

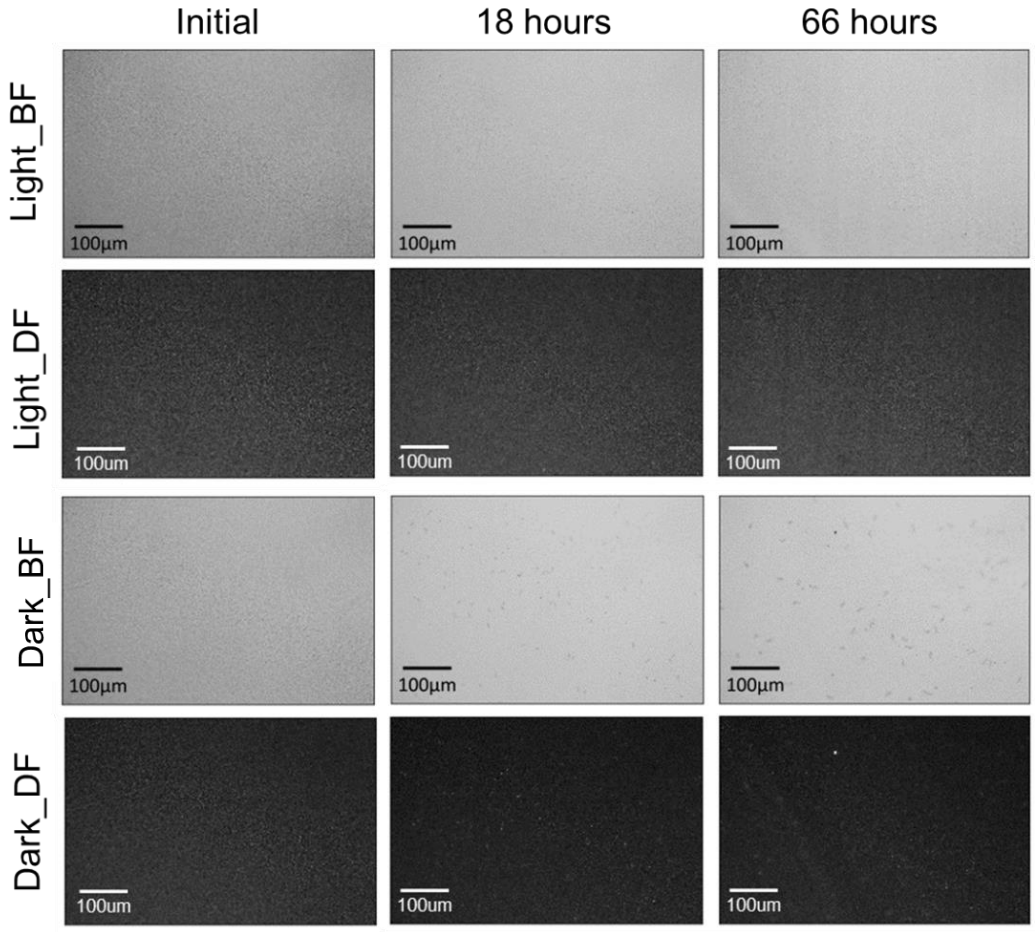

Figure 5. Secondary phases intensity tracking of $(FA_{0.83}Cs_{0.17})Pb(I_{0.86}Br_{0.14})_3$ perovskites during aging experiments in ambient environment conditions (40% RH, 25°C)

To qualitatively investigate those secondary phases we observed from microscopy BF and DF images (Figure 4, Figure 5), we applied XRD analysis on fresh and aged $(FA_{0.83}Cs_{0.17})PbI_3$ and $(FA_{0.83}Cs_{0.17})Pb(I_{0.86}Br_{0.14})_3$ samples. From Figure 6, $(FA_{0.83}Cs_{0.17})PbI_3$ aged under 0.25 Sun illumination (black trace) demonstrated no secondary phases peak was detected after 282 hours of aging under 40% Rh ambient environment at room temperature. Comparing with the pristine $(FA_{0.83}Cs_{0.17})PbI_3$ sample (purple trace), it shows nearly no difference in crystalline structure, thus indicating the crystalline structure of $(FA_{0.83}Cs_{0.17})PbI_3$ under 0.25 Sun illumination is stable after 282 hours of aging. On the other hand, δ-$CsPbI_3$ and δ-$FAPbI_3$ XRD peaks were detected from the $(FA_{0.83}Cs_{0.17})PbI_3$ control sample which aged in the dark for 282 hours. This result represented the crystalline structure of the sample which aged in the dark started transform from cubic phase perovskites crystalline structure to δ-$FAPbI_3$ and δ-$CsPbI_3$ phases during aging experiment and indicated that the perovskites crystalline structure is relatively unstable in the dark than under illumination. For $(FA_{0.83}Cs_{0.17})Pb(I_{0.86}Br_{0.14})_3$ perovskites, no secondary phases XRD peaks were observed for both illumination and dark conditions, which showing both samples are mainly containing α-(FACs)Pb(IBr). It indicates that incorporation of Br could effectively stabilizes the perovskites and prevents the formation secondary phases in FA-rich perovskites. Hence, based on result from sample $(FA_{0.83}Cs_{0.17})PbI_3$ and $(FA_{0.83}Cs_{0.17})Pb(I_{0.86}Br_{0.14})$ perovskite, we concluded that illumination and incorporation of Br showed the effect on suppressing the formation of secondary phases in perovskites and stabilized the crystalline structure of perovskites.

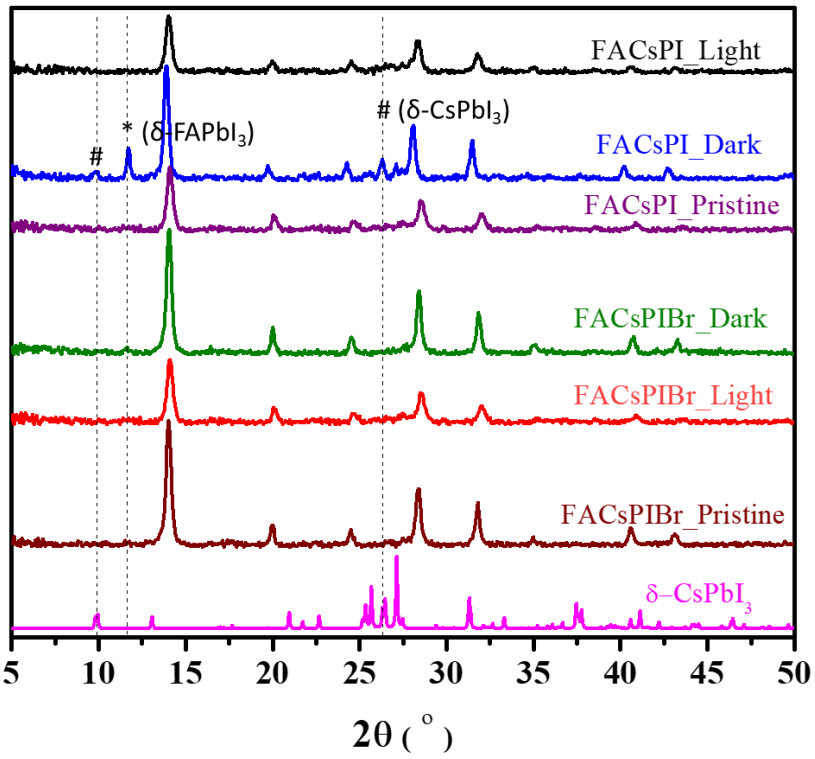


Figure 6. XRD patterns of pristine and aged $(FA_{0.83}Cs_{0.17})PbI_3$, $(FA_{0.83}Cs_{0.17})Pb(I_{0.86}Br_{0.14})_3$ perovskites samples at 40% RH for 282 hours, and δ-$CsPbI_3$ (COD #4518409) is provided for comparison.

3.4 Sub-bandgap Characterization of Perovskites Film

To quantify the sub-bandgap absorption of perovskites samples, we investigated $E_u$ from UV-Vis-NIR spectral data which collected from pristine perovskites samples. From Figure 7, $MAPbI_3$ showed the lowest $E_u$ of all compositions, indicating it has the lowest sub-bandgap absorption. However, for sample $(FA_{0.83}Cs_{0.17})PbI_3$, it presented the highest $E_u$. Moreover, we observed $E_u$ shares same increasing trend with microstrain which shown in Figure 2b. Thus, we believe the sub-bandgap absorption is highly related to microstrain, which implying it is strongly

related to lattice distortion of perovskites, even though sub-bandgap absorption is affected by many factors.

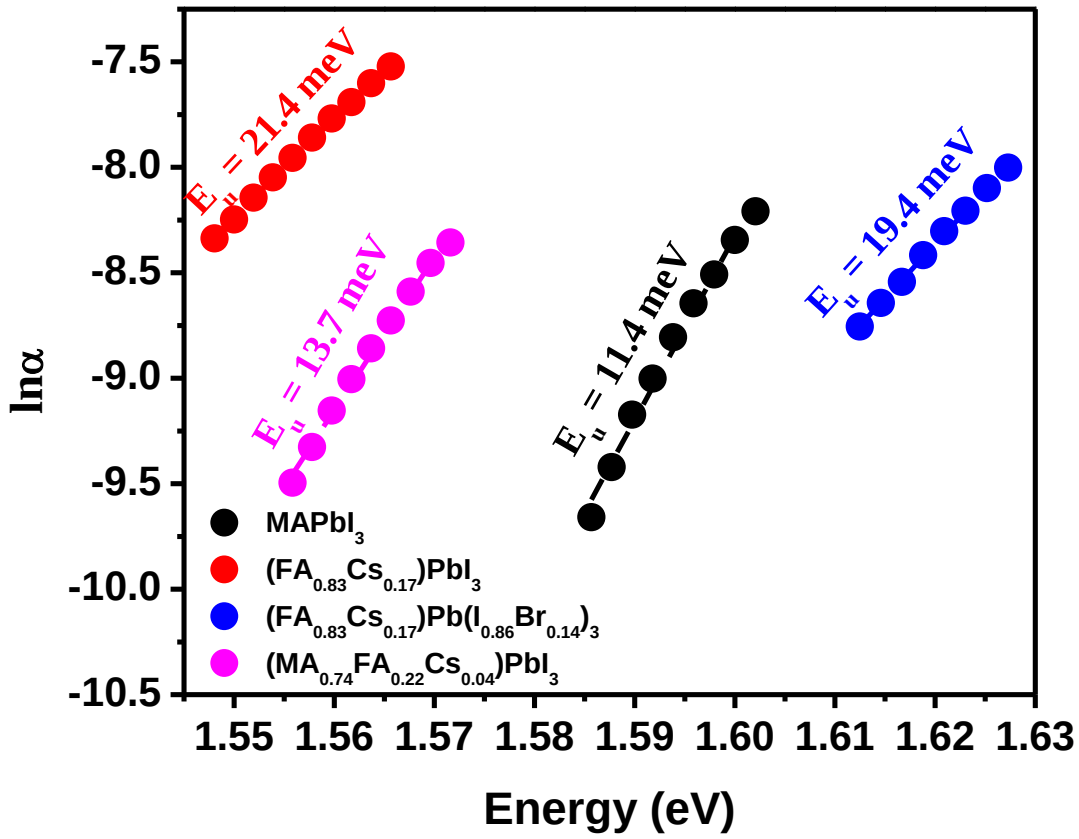


Figure 7. Urbach tail plots for spin-coated $MAPbI_3$, $(FA_{0.83}Cs_{0.17})PbI_3$, $(FA_{0.83}Cs_{0.17})Pb(I_{0.86}Br_{0.14})_3$, and $(MA_{0.738}FA_{0.217}Cs_{0.045})PbI_3$ perovskites films.

**4. Conclusion**

In summary, We fabricated different composition of perovskites and aged the film with 0.25 Sun illumination and in the dark respectively under ambient environment to investigate the degradation of perovskites and the formation of secondary phases. Through timeseries UV-vis-NIR and optical characterization result, we observed the photoactive perovskites degraded faster

while aged under 0.25 Sun illumination than in the dark for all compositions. To track the structural stability of (MA,FA,Cs)Pb(I,Br)$_3$ perovskites, we applied microscope with BF and DF capabilities during the aging experiment, and discovered FA-rich samples which aged under 0.25 Sun illumination showed less secondary phases than the control samples which aged in the dark. In order to confirm the observed secondary phases, we collected XRD data. We observed δ-CsPbI$_3$, and δ-FAPbI$_3$ XRD peaks only appeared in ($FA_{0.83}Cs_{0.17}$)PbI$_3$ which aged in the dark and no secondary phase peaks in ($FA_{0.83}Cs_{0.17}$)Pb($I_{0.86}Br_{0.14}$)$_3$ perovskites. To quantitatively study sub-bandgap absorption, we collected $E_u$ on the fabricated samples, and revealed that sub-bandgap absorption shares same increasing trend with the microstrain we observed from Williamson-Hall analysis in (MA,FA,Cs)Pb(I,Br)$_3$ perovskites. In this work, we provide a detailed research on the phenomenon of light-induced suppression on formation of secondary phases in FA-rich perovskites. We discovered that illumination and incorporation of Br can effectively suppress the formation of secondary phases and result in a more stable crystalline structure in FA-rich perovskites. The mechanism of this light-induced stabilization phenomenon is still needed to be elucidated, and we believe further research on it may be essential in improving the stability of perovskites PV.

## 5. References


1. Kojima, A., Teshima, K., Shirai, Y. &Miyasaka, T. Organometal halide perovskites as visible-light sensitizers for photovoltaic cells. *J. Am. Chem. Soc.* **131**, 6050–6051 (2009).
2. Sahli, F. *et al.* Fully textured monolithic perovskite/silicon tandem solar cells with 25.2% power conversion efficiency. *Nat. Mater.* **17**, 820–826 (2018).
3. Zuo, C. *et al.* Advances in perovskite solar cells. *Adv. Sci.* **3**, 1–16 (2016).

4. Hu, Z. *et al.* A Review on Energy Band-Gap Engineering for Perovskite Photovoltaics. *Sol. RRL* **3**, 1–9 (2019).
5. Kumawat, N. K. *et al.* Band Gap Tuning of CH3NH3Pb(Br1-xClx)3 Hybrid Perovskite for Blue Electroluminescence. *ACS Appl. Mater. Interfaces* **7**, 13119–13124 (2015).
6. Meng, L., You, J. &Yang, Y. Addressing the stability issue of perovskite solar cells for commercial applications. *Nat. Commun.* **9**, 1–4 (2018).
7. Hoke, E. T. *et al.* Reversible photo-induced trap formation in mixed-halide hybrid perovskites for photovoltaics. *Chem. Sci.* **6**, 613–617 (2015).
8. Aristidou, N. *et al.* The Role of Oxygen in the Degradation of Methylammonium Lead Trihalide Perovskite Photoactive Layers. *Angew. Chemie - Int. Ed.* **54**, 8208–8212 (2015).
9. Bryant, D. *et al.* Light and oxygen induced degradation limits the operational stability of methylammonium lead triiodide perovskite solar cells. *Energy Environ. Sci.* **9**, 1655–1660 (2016).
10. Christians, J. A., Miranda Herrera, P. A. &Kamat, P.V. Transformation of the excited state and photovoltaic efficiency of CH3NH3PbI3 perovskite upon controlled exposure to humidified air. *J. Am. Chem. Soc.* **137**, 1530–1538 (2015).
11. Yang, J., Siempelkamp, B. D., Liu, D. &Kelly, T. L. Investigation of CH3NH3PbI3degradation rates and mechanisms in controlled humidity environments using in situ techniques. *ACS Nano* **9**, 1955–1963 (2015).
12. Leijtens, T. *et al.* Towards enabling stable lead halide perovskite solar cells; Interplay between structural, environmental, and thermal stability. *J. Mater. Chem. A* **5**, 11483–11500 (2017).
13. Aristidou, N. *et al.* Fast oxygen diffusion and iodide defects mediate oxygen-induced

degradation of perovskite solar cells. *Nat. Commun.* **8**, 1–10 (2017).

14. Nagabhushana, G. P., Shivaramaiah, R. &Navrotsky, A. Direct calorimetric verification of thermodynamic instability of lead halide hybrid perovskites. *Proc. Natl. Acad. Sci. U. S. A.* **113**, 7717–7721 (2016).
15. Weber, O. J., Charles, B. &Weller, M. T. Phase behaviour and composition in the formamidinium-methylammonium hybrid lead iodide perovskite solid solution. *J. Mater. Chem. A* **4**, 15375–15382 (2016).
16. Boyd, C. C., Cheacharoen, R., Leijtens, T. &McGehee, M. D. Understanding Degradation Mechanisms and Improving Stability of Perovskite Photovoltaics. *Chem. Rev.* **119**, 3418–3451 (2019).
17. Ferdani, D. W. *et al.* Partial cation substitution reduces iodide ion transport in lead iodide perovskite solar cells. *Energy Environ. Sci.* **12**, 2264–2272 (2019).
18. Prochowicz, D. *et al.* Engineering of Perovskite Materials Based on Formamidinium and Cesium Hybridization for High-Efficiency Solar Cells. *Chem. Mater.* **31**, 1620–1627 (2019).
19. Lee, J. W. *et al.* Formamidinium and cesium hybridization for photo- and moisture-stable perovskite solar cell. *Adv. Energy Mater.* **5**, (2015).
20. Yin, W. J., Shi, T. &Yan, Y. Unusual defect physics in CH3NH3PbI3 perovskite solar cell absorber. *Appl. Phys. Lett.* **104**, (2014).
21. Chen, B., Yang, M., Priya, S. &Zhu, K. Origin of J-V Hysteresis in Perovskite Solar Cells. *J. Phys. Chem. Lett.* **7**, 905–917 (2016).
22. Chen, Y. &Zhou, H. Defects chemistry in high-efficiency and stable perovskite solar cells. *J. Appl. Phys.* **128**, (2020).

23. Marchezi, P. E. *et al.* Degradation mechanisms in mixed-cation and mixed-halide Cs: XFA1- xPb(BryI1- y)3 perovskite films under ambient conditions. *J. Mater. Chem. A* **8**, 9302–9312 (2020).

24. Johnston, A. *et al.* Bromine incorporation and suppressed cation rotation in mixed-halide perovskites. *ACS Nano* **14**, 15107–15118 (2020).

25. Han, F., Yang, W., Li, H. &Zhu, L. Stable High-Efficiency Two-Dimensional Perovskite Solar Cells Via Bromine Incorporation. *Nanoscale Res. Lett.* **15**, (2020).

26. Sharma, N. Optical band-gap and associated Urbach energy tails in defected AlN thin films grown by ion beam sputter deposition: Effect of assisted ion energyOptical band-gap and associated Urbach energy tails in defected AlN thin films grown by ion beam sputter depo. *Adv. Mater. Proc.* **2**, 342–346 (2017).

27. Greeff, C. W. &Glyde, H. R. Anomalous Urbach tail in GaAs. *Phys. Rev. B* **51**, 1778–1783 (1995).

28. Oheda, H. Change in the optical-absorption coefficient induced by optical modulation of the internal electric field in doping-modulated amorphous silicon multilayers. *J. Appl. Phys.* **67**, 6476–6480 (1990).

29. Ouyang, Y. *et al.* Photo-oxidative degradation of methylammonium lead iodide perovskite: Mechanism and protection. *J. Mater. Chem. A* **7**, 2275–2282 (2019).

30. Bush, K. A. *et al.* Compositional Engineering for Efficient Wide Band Gap Perovskites with Improved Stability to Photoinduced Phase Segregation. *ACS Energy Lett.* **3**, 428–435 (2018).

31. Stoddard, R. J. *et al.* Enhancing Defect Tolerance and Phase Stability of High-Bandgap Perovskites via Guanidinium Alloying. *ACS Energy Lett.* **3**, 1261–1268 (2018).

32. Williamson, G. K. &Hall, W. H. X-Ray broadening from filed aluminium and tungsten. *Acta Metall.* **1**, 22–31 (1953).

33. Li, C. *et al.* Methylammonium-Mediated Evolution of Mixed-Organic-Cation Perovskite Thin Films: A Dynamic Composition-Tuning Process. *Angew. Chemie - Int. Ed.* **56**, 7674–7678 (2017).

34. Gholipour, S. &Saliba, M. *Bandgap tuning and compositional exchange for lead halide perovskite materials*. *Characterization Techniques for Perovskite Solar Cell Materials* (Elsevier Inc., 2019). doi:10.1016/B978-0-12-814727-6.00001-3.

35. Cai, Y. *et al.* Tuning the A-site cation and X-site anion composition of CH3NH3PbI3 perovskite material for efficient planar perovskite solar cells. *Electrochim. Acta* **293**, 371–379 (2019).

36. J. Huang, S. T. et al. Impact of H2O on organic-inorganic hybrid perovskite solar cells. *Energy Environ. Sci.*, **10**, 2284 (2017).

37. Gratia, P. *et al.* The Many Faces of Mixed Ion Perovskites: Unraveling and Understanding the Crystallization Process. *ACS Energy Lett.* **2**, 2686–2693 (2017).